Path-integral Monte Carlo simulation of the structure of deuterium in the critical region

Martin Neumann
Institut für Experimentalphysik der Universität Wien, Strudlhofgasse 4, A-1090 Wien, Austria

Marco Zoppi
Consiglio Nazionale delle Ricerche, Istituto di Elettronica Quantistica, Via Panciatichi 56/30, I-50127 Firenze, Italy

(Received 15 February 1991)

The site-site distribution function and structure factor of deuterium close to the critical point have been calculated by means of quantum path-integral Monte Carlo simulations. The calculations were performed using a spherically symmetric pairwise-additive potential for the distribution of the molecular center of mass and assuming that D_2 may be regarded as a classical free rotor. Some of the problems connected with the simulation of a quantum system close to the critical point are analyzed in detail. The results of the simulations have been compared with the neutron-scattering experiment by Zoppi *et al.* [Phys. Rev. A **39**, 4684 (1989)]. The overall agreement is excellent, but some diffuse discrepancies are found. Possible origins of this inconsistency are discussed.

I. INTRODUCTION

In spite of the apparent ease with which liquid hydrogen may be investigated, it seems that the amount of experimental work devoted to this system, though quite extensive, is not commensurate to its importance. Probable reasons are of both theoretical and experimental origin. On the one hand, liquid hydrogen is a strongly quantum-mechanical system that renders any theoretical treatment extremely difficult. On the other hand, it also presents some intrinsic experimental difficulties that make this system not too appealing to experimentalists.

Determining analytically the microscopic dynamics of a liquid is already a hopeless problem for a classical system. For quantum fluids, the possibility of solving the Schrödinger equation for an N-body system seems even more remote. For classical fluids, computer simulations may provide the necessary link between theory and experiment. In particular, the molecular-dynamics (MD) technique, which solves Newton's equations for an N-particle system by numerical integration, allows one to obtain reliable information on the dynamical behavior of dense fluids. However, even though the technique has been used extensively to increase our knowledge of the liquid state in the classical framework, it has not yet evolved to a stage where the full dynamic N-body problem of a quantum liquid may be tackled.

The situation is quite different as far as the *static* properties of quantum fluids are concerned. In this case the Metropolis Monte Carlo (MC) technique, originally developed to compute classical equilibrium averages, has recently evolved into the path-integral Monte Carlo (PIMC) technique by means of which at least averages of equilibrium properties may now be evaluated quantum mechanically. For a review see, for example, Refs. [1] and [2].

On the experimental side, one of the problems is that x rays and neutrons, the most widely used sources of experimental information on liquids, are least effective with hydrogen. Since the molecule has only two electrons, the intensity of the scattered x rays is very low and experiments become difficult. On the other hand, the coherent cross section for thermal neutron scattering by hydrogen is almost two orders of magnitude smaller than the incoherent one, rendering this technique virtually useless for probing collective properties [3,4]. If deuterium is considered, however, the situation for thermal neutron scattering becomes much more favorable. The coherent cross section is now larger than the incoherent one and therefore collective properties of deuterium can be probed by this technique.

The structure factor of supercritical deuterium has recently been measured by neutron scattering using the pulsed neutron source of the Rutherford Appleton Laboratory (U.K.) [5]. The experiment was compared with MC simulations of a classical Lennard-Jones (LJ) system in a range of densities and temperatures roughly similar (with respect to the critical point) to the experimental conditions. The choice of a pairwise additive, spherically symmetrical, LJ potential might not seem unreasonable for a molecule such as D_2, but one can hardly expect that a classical simulation will quantitatively reproduce an experiment on a quantum-mechanical system. Moreover, due to the lack of extensive PVT data for deuterium, the equation of state of hydrogen had to be used to estimate the experimental densities. Nevertheless, the comparison between the experiment and the simulations was quite good on a *qualitative* level [5].

In order to bring the comparison to a *quantitative* level, progress had to be made in two directions. On the one hand, we found that extensive PVT data for deuterium, from which better estimates of the experimental densities and compressibilities could be obtained, were in fact available [6]. On the other hand, a PIMC program was developed to allow genuinely quantum-mechanical calculations of the structure factor. This program also used

TABLE I. Summary of the thermodynamic conditions for the experiment on gaseous deuterium. The densities and the compressibilities have been obtained from the *PVT* data given in Ref. 6. The critical parameters are $T_c = 38.34$ K, $P_c = 16.43$ atm, and $\rho_c = 10.43$ nm^{-3}.[a]

State	T (K)	p (atm)	ρ (nm^3)	χ_T (atm^{-1})
A	46.55	32.8	10.01	0.042
B	41.8	20.6	7.39	0.122
C	41.8	22.9	9.71	0.107
D	41.8	26.6	12.65	0.045

[a]H. M. Roder, G. E. Childs, R. D. McCarty, and P. E. Angerhofer, National Bureau of Standards Technical Note No. 641, 1973 (unpublished).

the "realistic" pair potential proposed by Norman, Watts, and Buck [7], rather than the simple 6-12 Lennard-Jones model. In this way it should now be possible to bring theory and experiment in quite close agreement.

The thermodynamic conditions of the experiment, which have been updated on the basis of the *PVT* data of Ref. [6], are given in Table I. For the comparison with the present simulation results we use the same structure factors that were reported in Ref. [5] (see also Ref. [8]). In Secs. II and III we give the details of the PIMC simulations. Since we are dealing with a system close to the critical point, the simulation results show a sizable dependence on the statistical ensemble as well as on the number of particles. These effects are discussed in Sec. IV. In Sec. V the simulations are compared with the experiment in both r space (Sec. V A) and Q space (Sec. V B). Finally, in Sec. VI we discuss the results and draw the conclusions.

II. MODEL POTENTIAL AND SIMULATIONS

In order to keep the computational effort within reasonable limits, our simulations were based on a number of simplifying assumptions. First, since D_2 is a weakly anisotropic molecule and may be regarded as a free rotor even in the condensed phase [9], the intermolecular potential was assumed to be spherically symmetric. This means that only the translational degrees of freedom had to be treated numerically, since the independent averaging over the rotational degrees of freedom yields a simple correction that may be added to the results later on. Thus the primary structural output of our simulations was the pair-correlation function for the molecular center of mass. Second, the intermolecular potential was assumed to be pairwise additive, i.e., irreducible three-body and higher-order interactions were neglected. They are probably not important for a weakly polarizable molecule such as D_2 [10]. Also, the experimental data with which the present simulation had to be compared are not sufficiently accurate (a precision much better than 1% would be required) to reveal such effects in the range of densities that is of interest here. Finally, in our quantum-mechanical calculations, exchange effects were considered to be negligible and the particles were assumed to obey Boltzmann statistics. This has been shown to be a good approximation for H_2 down to very low temperatures [11] and should *a fortiori* be true for D_2.

The pair potential we have used is that given by Norman, Watts, and Buck [7]. It is based on *ab initio* calculations as well as on a number of experimental gas and bulk phase properties and should give quite a realistic description of the energy surface. Only the spherically symmetric component was used in the present calculations. The collision diameter and well depth of this potential are $\sigma = 3.001$ Å and $\varepsilon/k_B = 33.833$ K, respectively, which may be compared with the traditional Lennard-Jones values $\sigma_{LJ} = 2.959$ Å and $\varepsilon_{LJ}/k_B = 36.7$ K [12].

With that potential we have performed Monte Carlo simulations in the classical canonical (MC) and grand-canonical (GCMC) ensemble as well as path-integral Monte Carlo (PIMC) simulations in the quantum-mechanical canonical ensemble. In all these calculations the particles were confined to a cubic box with volume V and edge length $L = V^{1/3}$, to which periodic boundary conditions were applied. Density and temperature were chosen in accordance with the experimental conditions given in Table I. Intermolecular interactions were truncated spherically at $r_c = L/2$ and internal energies and pressures were corrected in the usual way by integrating over a uniform particle density beyond the cutoff.

All simulations were based on the Metropolis algorithm [13] and single-particle trial moves in which the center of mass of a randomly chosen molecule was displaced randomly within a small cube of edge length $D = 4.0$ Å (the same value of D was used for all simulations). Most of the simulations consisted of 50 000–100 000 attempted moves per particle (passes), after an extensive equilibration phase. The initial configuration was usually taken from the end of a previous run.

In the PIMC simulations we have used the "primitive algorithm" [14]. The number of beads on the ring polymers that, in the classical ismorphism, is equivalent to the quantum particles, was varied between $P = 4$, 8, and 16. A trial move consisted of a random displacement of the "center of mass" of the polymer and a new set of "intramolecular coordinates" that were sampled directly from the free-particle density matrix (a multivariate Gaussian). This is a very efficient algorithm, as long as the actual distribution of "intramolecular coordinates" is not too different from the free-particle case, since it allows one to use the same maximum displacement for the "center of mass" as for the classical one to use the same maximum displacement for the "center of mass" as for the classical system (cf. the acceptance ratios x_A in Table II).

In the GCMC simulations, a trial move was, with an *a priori* probability of $\frac{1}{3}$ each, either an attempt to insert or delete a particle or a random displacement of an existing particle. Since, in the grand-canonical ensemble, the number of particles is not constant but determined by the value of the chemical potential, the volume was chosen to be the same as in the canonical simulations with $N = 64$, 256, or 1024 particles, and the (excess) chemical potential

was adjusted until the average density settled down close to the desired value. This worked quite well, except for the largest system where this method of trial and error was too time consuming.

The details of the simulations as well as some thermodynamic results are summarized in Table II. R is the radius of gyration of the ring polymers in the PIMC algorithm, i.e., the "spread" of the quantum particles. It is generally less than 10% of the classical collision diameter, indicating that in these systems quantum effects will be appreciable but not overwhelming. Note also that the acceptance ratio x_A (i.e., the fraction of accepted trial moves) in PIMC is about the same as in the classical simulations. The kinetic energies (and pressures) reported in Table II have been calculated using the so-called "crude energy estimator" [15].

III. CONVERGENCE TO THE QUANTUM-MECHANICAL LIMIT

The essence of the PIMC method is that, in principle, exact quantum-mechanical results may be obtained from

TABLE II. Details of simulations and thermodynamic properties of D_2 in the critical region. N is the number of molecules, P is the number of beads on the ring polymers (Trotter number), x_A is the fraction of accepted trial moves (acceptance ratio), and R is the root-mean-square spread of the ring polymers (radius of gyration). The maximum displacement was $D=4.0$ Å in all simulations. We report the results of the translational kinetic energy per molecule E_{tr}, the potential energy U, the excess chemical potential μ^{ex}, the pressure p, and the isothermal compressibility χ_T.

State	Method	$N(\times P)$	Passes (10^3)	x_A	R (Å)	E_{tr} (K)	U (kJ/mol)	μ^{ex} (kJ/mol)	p (atm)	χ_T (atm^{-1})
A										
	MC	64	100	0.350		69.825	−0.5552		23.0	
		256	100	0.341		69.825	−0.5753		23.2	
		1024	50	0.335		69.825	−0.5883		23.0	
	GCMC	64.6[a]	1000	0.144[b]		69.825	−0.6120	−0.526	27.1	0.14
				0.122[c]						
		254.9[a]	1000	0.112[b]		69.825	−0.6063	−0.539	23.9	0.34
				0.118[c]						
		998.7[a]	40	0.112[b]		69.825	−0.5862	−0.535	23.1	0.60
				0.116[c]						
	PIMC	64×16	100	0.352	0.252	74.9	−0.5123		30.6	
		256×8	50	0.345	0.250	75.1	−0.5256		31.0	
		1024×8	20	0.343	0.250	75.3	−0.5269		31.5	
B										
	MC	64	100	0.405		62.7	−0.4507		15.8	
		256	100	0.392		62.7	−0.4783		15.1	
	PIMC	64×16	100	0.421	0.266	66.6	−0.4015		20.0	
		256×8	50	0.412	0.264	67.0	−0.4168		19.9	
C										
	MC	64	100	0.330		62.7	−0.5646		13.2	
		256	100	0.313		62.7	−0.6022		13.0	
		1024	50	0.292		62.7	−0.6596		12.7	
	PIMC	64×4	100	0.336	0.256	67.2	−0.5178		19.5	
		64×8	100	0.338	0.264	67.8	−0.5130		20.3	
		64×16	100	0.338	0.266	68.0	−0.5116		20.6	
		256×8	50	0.329	0.264	68.0	−0.530		20.6	
D										
	MC	64	100	0.256		62.7	−0.7025		6.1	
		256	100	0.243		62.7	−0.7361		8.5	
	PIMC	64×16	100	0.254	0.265	70.0	−0.6458		20.5	
		256×8	50	0.249	0.263	69.8	−0.6602		20.7	

[a]Average number of particles. The resulting density in these simulations was $\rho=10.10$, 9.97, and 9.76 nm^{-3}.
[b]Particle insertions or deletions.
[c]Random displacements

purely classical calculations in the limit that the number of beads on the ring polymers, P, goes to infinity. In practice this means that either P has to be increased until the results do not change any more or one has to find a way of extrapolating the results obtained with a finite number of beads.

We have investigated the convergence to the quantum-mechanical limit, $P \to \infty$, for a system of $N=64$ particles at the thermodynamics state C, by performing simulations with $P=4$, 8, and 16 beads. As can be seen from Table II, the kinetic and potential energies as well as the pressure are still dependent on P, but when plotted as a function of $1/P$ they virtually fall on a straight line, so that an extrapolation to $1/P \to 0$ is straightforward (cf. also Ref. [16]). For the 64-particle system at state C the extrapolated values found in this way are $E_{\rm tr}/k_B = 68.3$ K for the kinetic energy per particle and $p = 20.9$ atm for the pressure. Since, at fixed P, kinetic energy and pressure also do not depend strongly on the number of particles, it is probably safe to say that, for all thermodyanmic states considered here, the results obtained from the PIMC simulations with the largest N are, within 1–2 K and 1–2 atm, respectively, those of the infinite quantum-mechanical system.

In Table II the translational kinetic energies are generally found to be some 20% higher than the classical value of $\frac{3}{2}k_B T$. Quantum effects are also important for the pressure, which is considerably raised above the values obtained with a classical simulation. On the whole, the agreement between the calculated pressures and the experimental values is very good (whether the slight discrepancy for state D, where the quantum corrections are largest, is an artifact of the simulation or is due to the experimental conditions not having been established accurately enough is not clear to us).

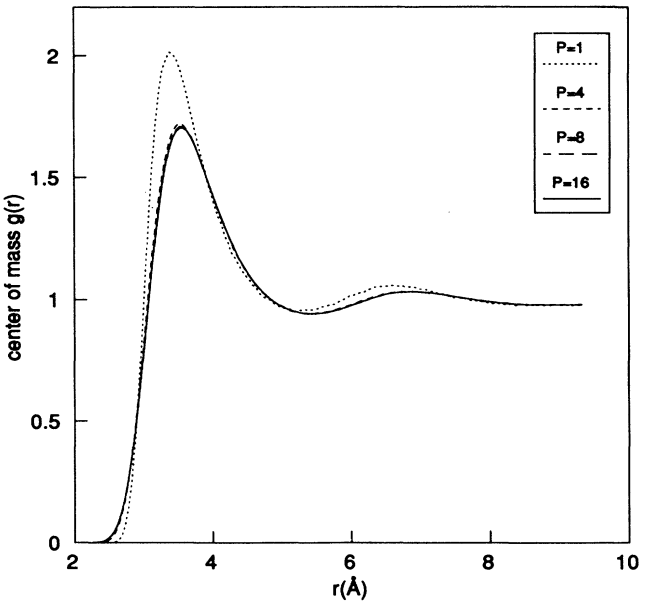

FIG. 1. Dependence of $g(r)$ on the number of beads for state C. The number of particles was $N=64$ in all simulations and the number of beads was $P=1$ (classical), 4, 8, and 16 (top to bottom). The curves for $P=8$ and 16 are indistinguishable on the scale of the graph.

The dependence of the pair-correlation function on P is shown in Fig. 1. There, we have plotted the pair-correlation function $g(r)$ of a classical system of 64 particles at state C along with the PIMC results using $P=4$, 8, and 16 beads. It can be seen that the influence of quantum effects is profound, resulting in a general outward shift of the peaks, a significant lowering of the first peak, some loss of structure around the second peak, and an effective softening of the repulsive interaction. More importantly, the curves for $P=8$ and 16 are indistinguishable on the scale of the graphs so that, at least for a visual inspection, the quantum-mechanical limit of $g(r)$ has already been reached. Therefore, in our later PIMC simulations of larger samples, we have usually worked with $P=8$ beads.

IV. DEPENDENCE ON THE NUMBER OF PARTICLES

From Fig. 1 it can be seen that the quantum correction to $g(r)$, i.e., the difference between the quantum-mechanical and the classical curve is largest around the first peak and decreases with increasing distance. We also knew, from our previous work with the Wigner-Kirkwood expansion, that in fluids these corrections to $g(r)$ are of short range [17]. Therefore, our original intention had been to calculate the quantum corrections for a small system (say $N=64$) and to add them to the correlation function obtained from a classical calculation of larger systems. That we would eventually have to use large samples was clear from the outset, because when the system is very close to the critical point $g(r)$ may be expected to exhibit a sizable N dependence as well as the onset of the long-range tail associated with the large compressibility of the real system.

In the present case, however, there is the additional difficulty that simulations of a hypothetical classical D_2 fluid, at the thermodynamic states considered here, would actually be in the two-phase region. This is best illustrated by means of Fig. 2, where the location of the experimental states $A-D$ (circles) is shown relative to the coexistence line of D_2 [6]. (Note that reduced units with respect to the critical parameters have been used in this figure). By "turning off" quantum mechanics [18], these points move below the coexistence line, into the two-phase region (squares).

We have nevertheless performed a series of classical simulations since, for a small system, the homogeneous phase will be metastable and might still be useful as a reference system. These simulations were carried out in the canonical as well as in the grand-canonical ensemble, and although they did not turn out to be useful in the end, we will briefly describe some results since there does not seem to be much known about the behavior of $g(r)$ in this region of the phase diagram (see Ref. [19], however), especially in the grand-canonical ensemble.

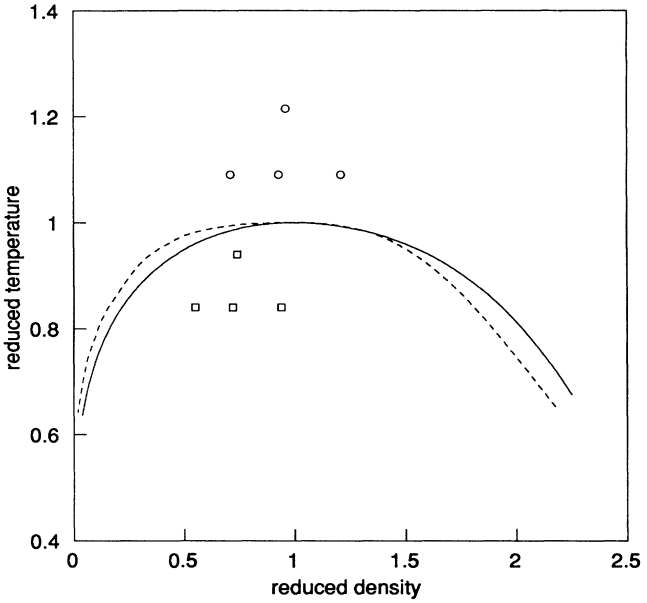

FIG. 2. Thermodynamic states of D_2 in the ρ-T plane, in units reduced with respect to the critical parameters. The circles indicate the real location of the experiment, while the squares represent the classical simulations. The solid and dashed lines are the coexistence lines for D_2 [6] and for a classical Lennard-Jones system [18].

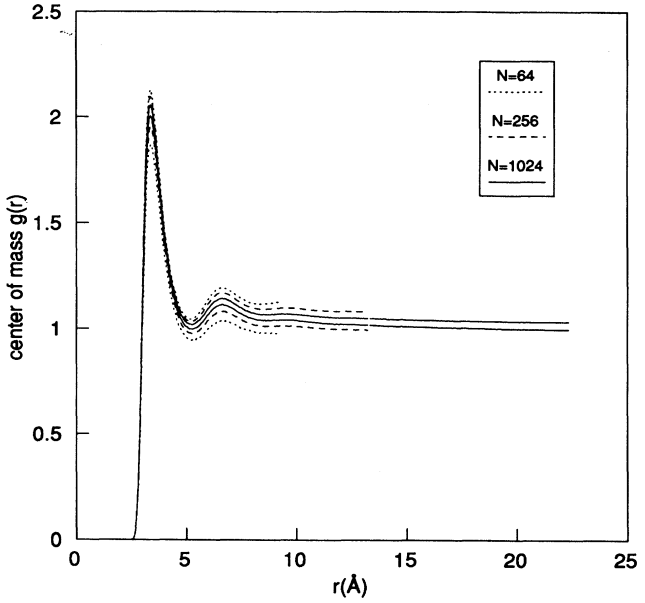

FIG. 3. N dependence of $g_{\text{c.m.}}(r)$ for classical simulations in the canonical (MC, lower curves) and grand-canonical ensemble (GCMC, upper curves) at state A. The number of particles is 64, 256, and 1024. (MC, bottom to top; GCMC, top to bottom).

A. Classical simulations: MC and GCMC

Figure 3 shows the pair-correlation functions obtained from canonical (MC) and grand-canonical (GCMC) simulations of classical systems of various sizes at state A. In the MC simulations the number of particles was $N=64$, 256, and 1024, and the resulting box sizes were also used in the GCMC simulations while the chemical potential was adjusted such as to give approximately the same number of particles. From the figure it is evident that, in contrast to liquids near the triple point. $g(r)$ exhibits a tremendous N dependence in this region of the phase diagram, and so these simulations were of no practical use. Interestingly, the MC results show a tendency to increase, and the GCMC results tend to decrease, as the number of particles is increased, and the two sets of curves seem to bracket some kind of limiting behavior. In practice, this limit will not be reached until the system is large enough to separate into two phases, and the resulting $g(r)$ will be just an average correlation function for the coexisting liquid and gaseous phases [20].

At finite N, the correlation function for the canonical ensemble (MC), which is constrained to the homogeneous phase by the periodic boundary conditions, does seem to develop the long-range tail expected in the critical region but is eventually forced to fall below 1.0, due to the normalization of $g(r)$ to the number of particles in the box. On the other hand, in the grand-canonical ensemble (GCMC), which effectively samples both phases, the density fluctuations are unrealistically high in the two-phases region (cf. the entries for χ_T in Tables I and II), and therefore $g(r)$, which in this ensemble is normalized to the compressibility, is significantly above 1.0 at long range.

B. Quantum-mechanical simulations: PIMC

As soon as quantum mechanics is "turned on," and provided that the potential of Norman, Watts, and Buck is a reasonable model for D_2, our thermodynamic states will move to the correct side of the coexistence line in the phase diagram of Fig. 2, and the only problems encountered in the simulations should be those associated with the proximity of the critical point.

The situation for state A is shown in Fig. 4, where we have plotted the pair-correlation function obtained from canonical PIMC simulations using $N=64$, 256, and 1024 particles. It can be seen that the N dependence is still appreciable, but the situation is considerably improved as compared to the classical case. Now the difference between the 1024- and the 256-particle system is much less than that between the 256- and 64-particle system, and it is probably safe to say that $g(r)$ for an infinite system would lie only slightly above the $N=1024$ result, at least at small and intermediate r. The larger system also nicely shows the buildup of the critical tail, although the curves cannot be trusted for large r where they again fall slightly below 1.0 for the reasons already indicated in the preceding section.

The quantum corrections, defined as the difference between the quantum-mechanical and classical $g(r)$, turn out to be very sensitive to the number of particles and are not short ranged, since they have to compensate for the incorrect behavior of the classical results at long range.

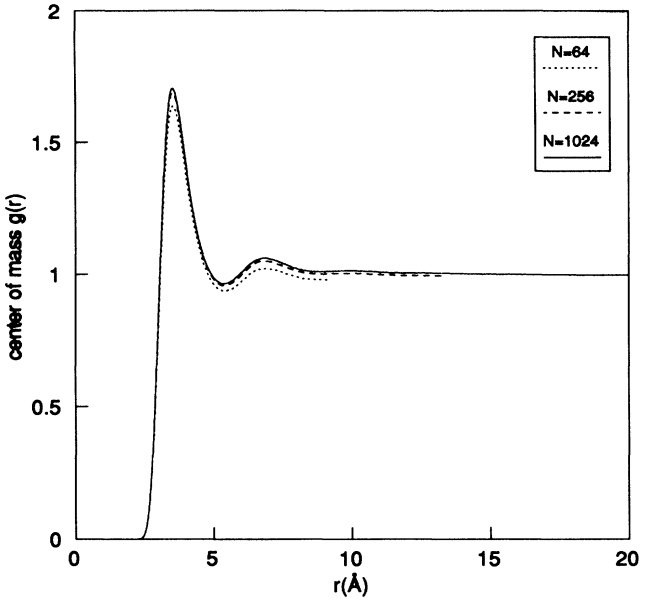

FIG. 4. N dependence of $g(r)$ for quantum-mechanical canonical PIMC simulations at state A. (Top to bottom: $N=1024$, 256, and 64).

Thus a full quantum-mechanical simulation seems to be indispensable, and perturbation methods that, like the Wigner-Kirkwood expansion [21], rely on the classical reference system, are bound to fail in this region of the phase diagram.

All things considered, our "best" simulations (i.e., using $P=8$ beads and $N=256$ or 1024 particles), being close to the quantum-mechanical limit and probably within 1–2 % of the infinite system result up to intermediate distances, should be sufficiently accurate to allow a critical assessment of the experimental data in the following section.

V. COMPARISON WITH THE EXPERIMENT

The principal structural output from our PIMC simulations is the pair-correlation function $g(r)$. Since the simulations were performed using a spherical particle model, this is actually the correlation function of the center of mass, $g_{\text{c.m.}}(r)$, while the experiment probes the atom-atom correlation function $g_{a\text{-}a}(r)$. In order to connect the two quantities, it is necessary to discuss briefly the rotational dynamics of hydrogen.

It is well known that, even in the low-pressure solid, the hydrogen molecule behaves like a free rotor [9]. This is a direct result of the anisotropic contribution to the interaction potential being very small compared to the isotropic component. Since the density of deuterium in the critical region is about three times smaller than that of the solid at the triple point, it seems reasonable to assume that a quantum-mechanical free-rotor model is a very good approximation of the real behavior of our sample.

The theory can be made even simpler, however. Sears has shown that when the ortho-para concentration is the same as in the infinite temperature limit (normal concentration), the dependence of the neutron cross section on particle statistics (Bose-Einstein or Fermi-Dirac) reduces to Boltzmann statistics [22]. In addition, if no vibrational transitions are taken into account (and the Debye-Waller factor is neglected), and if the energy of the incoming neutrons is larger than all energy transfers giving an appreciable contribution to the cross section, then the molecular cross section for elastic scattering reduces to that of a *classical* free rotor [22].

Therefore, since the neutron experiment was performed within a limited amount of time (3 days, using a vanadium container, which is not expected to catalyze the ortho-para conversion) and since the distribution of incoming neutrons was centered at an energy appreciably higher than the first few rotational transitions, we will assume that the classical free-rotor model applies to deuterium in the present experimental conditions.

This assumption leads to the following relationship between the structure factors [23]:

$$[S_{a\text{-}a}(Q)-1]=f_1(Q)+f_2(Q)[S_{\text{c.m.}}(Q)-1]\ , \tag{1}$$

where $S_{a\text{-}a}(Q)$ and $S_{\text{c.m.}}(Q)$ are the atom-atom and center-center structure factors,

$$f_1(Q)=\tfrac{1}{2}(\sin Qd)/(Qd)\ , \tag{2}$$

$$f_2(Q)=[(\sin Qd/2)/(Qd/2)]^2 \tag{3}$$

and $d=0.748\,35$ Å [24] is the intramolecular distance of D_2. By Fourier transforming $g_{\text{c.m.}}(r)$ and using Eq. (1), it is now possible to calculate an atom-atom structure factor from the simulation, which may be compared with the corresponding experimental function.

Since $[S(Q)-1]/r$ and $[g(r)-1]$ are Fourier-transform pairs, the comparison may also be performed in r space. Here, the equivalent of Eq. (1) [apart from a δ function corresponding to the intermolecular term $f_1(Q)$] is the convolution integral (see the Appendix for a derivation)

$$g_{a\text{-}a}(r)=1+(1/rd^2)\int_{r-d}^{r+d} dR\ R[g_{\text{c.m.}}(R)-1] \times(d-|R-r|)\ . \tag{4}$$

Either way, the comparison is best performed on the atom-atom functions, since division of the experimental structure factor by $f_2(Q)$ leads to very large uncertainties near the zeros of the latter function.

A. Comparison in r space

Structural data may be compared either in r space or in Q space. Working in r space, where correlations are easier to visualize, requires the inverse Fourier transform of the experimental structure factor. This means that $S(Q)$ has to be extrapolated somehow beyond the range in which it has been measured. Otherwise, also because of statistical errors, spurious oscillations may occur at small r. The maximum-entropy (ME) simulation procedure [25], now better known as the reverse Monte Carlo (RMC) method [26], has been introduced just to circumvent this problem. Here, only the available experimental points (weighted by their individual errors) and

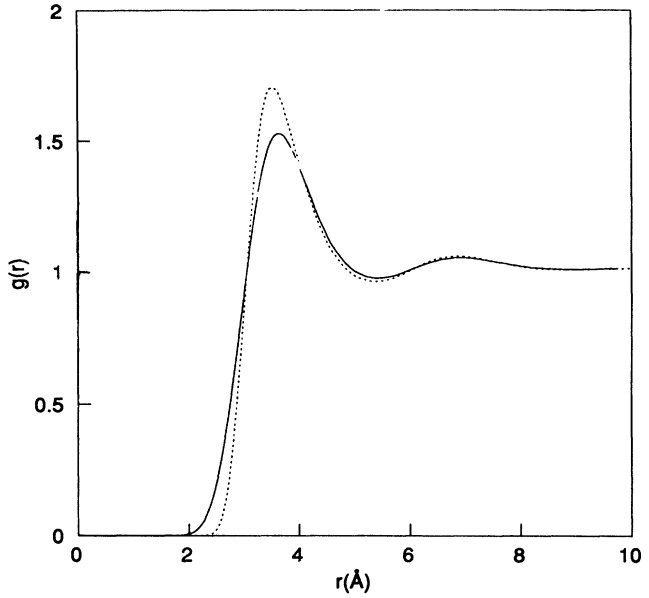

FIG. 5. Evolution of $g_{c.m.}(r)$ (dotted line) into $g_{a\text{-}a}(r)$ (solid line) at state A (PIMC, $N=1024$).

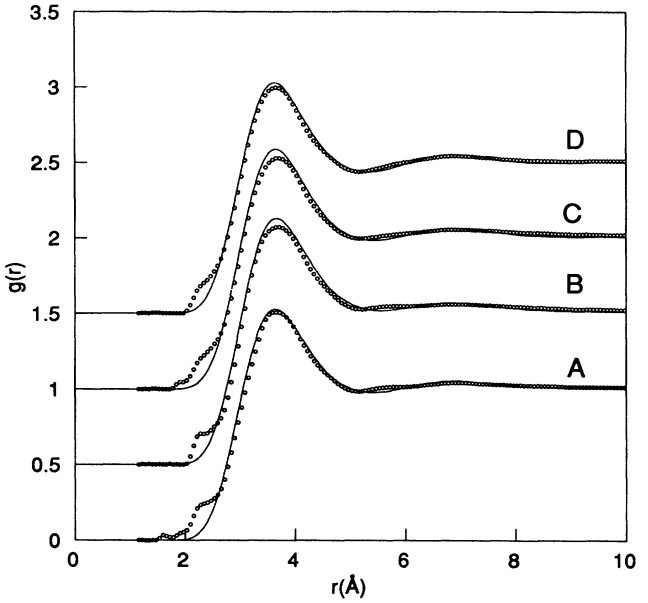

FIG. 6. Comparison between simulation (solid line) and experiment (circles) for the site-site correlation function $g_{a\text{-}a}(r)$. The curves have been shifted for clarity. The thermodynamic states are labeled according to Table I.

the measured compressibility are used [5]. The experimental site-site correlation function shown in Fig. 6 have been obtained in this way.

In the simulation results, $g_{a\text{-}a}(r)$ was calculated from $g_{c.m.}(r)$ by means of Eq. (4). The effect of this convolution is shown in Fig. 5 for the thermodynamic state A. The foot of $g_{a\text{-}a}(r)$ extends to much smaller distances than that of $g_{c.m.}(r)$, and the first peak shifts slightly outward and decreases by more than 10%. At long range the differences decrease and disappear completely beyond the second peak. Qualitatively, this is very similar to the effect of "switching on" quantum mechanics on a classical $g(r)$ (cf. Fig. 1), except that for the thermodynamic states considered here the quantum effects are of longer range.

Figure 6 shows the comparison between experiment and simulation for the four thermodynamic points, which are labeled A, B, C, and D, in Table I. The best agreement between theory and experiment is obtained for state A. There, short- and long-range behavior of the correlation function are reproduced extremely well, and the peak height is off by only 1.5%. The agreement is less perfect for the other three states, although still quite satisfactory even on a quantitative basis. We tend to attribute this behavior to the fact that state A is the one with the highest temperature, i.e., the most distant from the critical point, which should therefore be more well behaved. It is certainly not due to the greater number of particles (1024), since increasing N generally raises the curves (cf. Fig. 4), and this would *worsen* the situation for states B, C, and D.

Concerning the long-range behavior, we note that the experimental data are always above 1.0 while the simulations tend to fall below this value. For the experimental curves this effect is probably due to the use of slightly exaggerated values for the compressibilities (cf. Table I of Ref. [5] and Table I of the present work) in the ME fit. The "unphysical" long-range behavior of the simulated curves is a size effect, since only 256 particles were used in states B, C, and D, and the correlation functions in the canonical ensemble are not normalized to the compressibility (cf. Sec. IV B).

Finally, we note that there is a general oscillatory behavior of the experimental functions around the simulation results. This is most evident at short range, where all of the curves show a marked structure at the foot of the $g_{a\text{-}a}(r)$, but there is also a small hump after the first minimum. Both features are definitely not real, and since the invariably low values of the first peak may also be an artifact of the ME procedure, we will also analyze our results in Q space.

B. Comparison in Q space

Moving from r space to Q space transforms the difficulties as well. Now it is the simulation results that have to be Fourier transformed, and since correlation functions may only be calculated up to half the box length, there will again be truncation effects. In principle, there is the possibility of extending the data by using an approximate integral equation [2,12] or a similar approach, but this did not seem sensible in the present case where the data are already affected by finite-size effects at long range. Thus, the procedure adopted here was to simply truncate the integrals at a convenient point and to ignore the results for Q values smaller than $Q_{\min}=2\pi/L$, where L is the box length. Depending on the size of the system ($N=1024$ or 256), $Q_{\min}$ is of the order of 0.1–0.2 Å^{-1}. At the other end of the Q range ($Q \geq 4$–5 Å^{-1}), the structure factor is dominated by intramolecular

correlations, but, for the sake of completeness, we will plot our results up to twice this limit.

Figure 7 compares the experimental atom-atom structure factor $S_{a\text{-}a}(Q)$ with that obtained by means of Eq. (1) from the simulations. The overall agreement is extremely good, especially if we consider that no adjustable parameters have been used in the calculations. For $Q \to 0$ all curves show the increasing behavior associated with the high values of the compressibility, although there the simulation results should be taken with caution. The subsequent minimum is reproduced very well at state A, but the simulation results are slightly higher than the experimental values for states B, C, and D. In the region of the peak the situation is reversed, with a slight discrepancy at state A and much better agreement for the other three states. Finally, for $Q \geq 4\text{–}5$ Å^{-1}, where the structure factor is mainly determined by the intramolecular contribution, the scatter of the experimental points around the theoretical curves seems to be more or less consistent with the statistical error of the data.

In order to have a quantitative measure for our observations, we have also calculated a reduced χ^2 defined as

$$\chi_R^2 = (1/M) \sum_{i=1}^{M} [S_{\text{expt}}(Q_i) - S_{\text{calc}}(Q_i)]^2 / \sigma_{\text{expt}}^2(Q_i) , \tag{5}$$

where M is the number of data points used in the comparison. The results are summarized in Table III. The values of the χ_R^2 are much too high if the entire Q range (0.2–10.0 Å^{-1}) is considered, but may be drastically reduced by omitting the data below $Q_{\min} = 0.6$ Å^{-1}. However, they increase again if we also disregard the data above $Q_{\max} = 5.5$ Å^{-1}, where the intermolecular contribution becomes insignificant. Therefore, in spite of the remarkable visual agreement, the values of χ_R^2, which should be of the order of 1, never become smaller than 7.

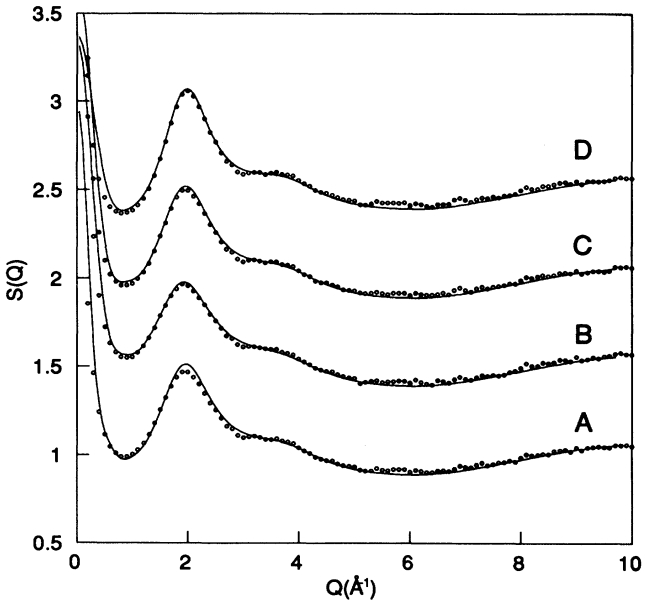

FIG. 7. Comparison between simulation (solid line) and experiment (circles) for the site-site structure factor $S_{a\text{-}a}(Q)$. The curves have been shifted for clarity. The thermodynamic states are labeled according to Table I. The experimental statistical errors are smaller than the size of the symbols.

TABLE III. Reduced χ^2 for the comparison in Q space.

State	χ_R^2 [a]	χ_R^2 [b]	χ_R^2 [c]
A	93	9.0	14.9
B	119	7.2	10.7
C	231	11.3	18.6
D	230	26.2	44.6

[a] $Q_{\min} = 0.2$ Å^{-1}; $Q_{\max} = 10$ Å^{-1}; $M = 99$.
[b] $Q_{\min} = 0.6$ Å^{-1}; $Q_{\max} = 10$ Å^{-1}; $M = 95$.
[c] $Q_{\min} = 0.6$ Å^{-1}; $Q_{\max} = 5.5$ Å^{-1}; $M = 50$.

There may be a number of reasons why the values of χ_R^2 are so high, and these are both of experimental and theoretical origin. First of all, we recall the experimental densities are somewhat uncertain because of a likely error in the true temperature of the sample in the scattering volume [5]. If the true temperatures were higher than the measured ones, this would decrease the densities with respect to the values of Table I. As a consequence, the theoretical $[S_{a\text{-}a}(Q) - 1]$ would also decrease while at the same time the experimental points would be increased. This could close the gap in the peak region of $S_{a\text{-}a}(Q)$ for state A without changing the function too much where it is close to unity. However, such a large correction would destroy the quite satisfactory agreement in this region for states B, C, and D. Also, a density correction would probably not improve the situation around the minimum of $S_{a\text{-}a}(Q)$.

On the theoretical side, the principal limitation of any simulation is the intermolecular potential, which, in general, is only imperfectly known. The calculated pressures were quite reasonable, but it is not clear whether the potential of Norman, Watts, and Buck is a faithful representation of D_2, especially if anisotropic and many-body contributions are ignored. Our calculations were also affected by certain size effects, but with the present limitations on the accuracy of the experimental data, more extensive simulations would not have been justified.

Another possible source of error is the assumption that D_2 may be treated as a classical free rotor. This was based on a calculation by Sears [22], followed by a number of additional hypotheses (see above). However, this may involve quite drastic approximations. For example, even if the peak of the incoming neutron distribution is of sufficiently high energy to excite many rotational transitions, so that the quantum free-rotor cross section reduces to the classical one, there may still be enough energy in the tails of the distribution to also induces some vibrational transitions, and so the approximation may fail.

All of these effects should be checked more carefully, in particular how, and by how much, the details of the molecular cross section affect the measured structure factor. This is feasible, but beyond the scope of the present work [27].

VI. CONCLUSIONS

Apart from the very good agreement obtained between the experimental results and the simulations, there are a number of things that we have learned from the present work. First, and not unexpectedly, simulations in the critical region are a rather delicate matter and should be performed and interpreted with the necessary care, even at temperatures as much as 20% higher than the critical point. In particular, it is difficult to imagine that the use of perturbation theory to evaluate quantum corrections in this region could give sensible results if, as in Fig. 2, the (classical) reference system is in an unstable thermodynamic state. With PIMC this is not a problem, since for sufficiently large P the system should be close to its true thermodynamic state.

Our simulations were also affected to some extent by finite-size effects, which are quite appreciable in a rather wide region around the critical point. The accuracy of the experimental results did not really justify more extended calculations. However, on the basis of the present experiences and using neighborhood tables and/or link cells [2] (and reducing the interaction range), it would not be too difficult to perform even grand-canonical PIMC simulations on systems of several thousand particles. These would give very accurate theoretical predictions but should be linked to a corresponding improvement of the experimental situation.

Unfortunately, for the present set of data the experimental conditions are not as well defined as would be desirable for a very accurate comparison. As mentioned in the experimental report in Ref. [5], due to leakage in the vacuum tank of the neutron spectrometer, a temperature gradient was measured between the top and bottom of the scattering cell and therefore the densities are not known with sufficient accuracy. From an experimental point of view, a small density change may be fully neglected, as far as the standard corrections to the data are concerned, and this will only affect the measured structure factor by a constant multiplicative factor (cf. Fig. 7, where a slight adjustment of the data might increase the quality of the agreement and reduce drastically the value of χ_R^2). In order to estimate the magnitude of this effect on the simulation data, we have repeated the (classical) simulation of state C at the highest plausible value of the temperature of the sample (43 K, with a consequent change in the density from 9.71 to 7.9 nm^{-3}). From Fig. 8 we find that the simulation results for the center-of-mass correlation function do not change very much (though in the right direction) and this, by itself, seems to be insufficient to explain the discrepancy in the region between 5 and 8 Å.

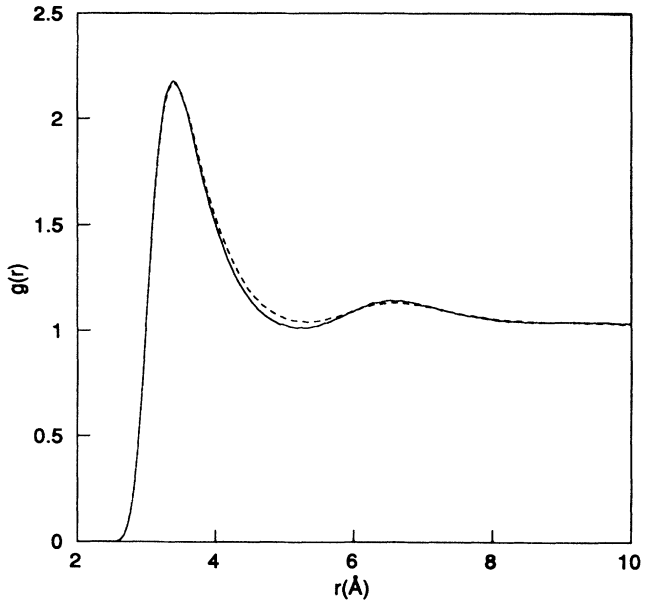

FIG. 8. Change of the *classical* center-of-mass correlation function $g_{\text{c.m.}}(r)$ for state C, due to possible uncertainties in the experimental conditions. The curves have been obtained from classical MC simulations using $N=256$ particles. The solid line corresponds to the choice $T=41.8, \rho=9.71$ nm^{-3} and the dashed line to $T=43.0, \rho=7.90$ nm^{-3}. For both states the experimental pressure is 22.9 atm.

ACKNOWLEDGMENTS

The simulations reported here have been performed on various computers at the Prozessrechenanlage Physik der Universität Wien and at the Bundesministerium für Wissenschaft und Forschung, Wien. We would like to thank A. K. Soper for helpful and stimulating discussions.

APPENDIX

For isotropic fluids, the 3D Fourier transform that relates the pair-correlation function $g(r)$ to the structure factor $S(Q)$ [23],

$$S(Q)-1=\rho\int d\mathbf{r}[g(r)-1]\exp(i\mathbf{Q}-\mathbf{r}) , \tag{A1}$$

reduces to the 1D integral

$$S(Q)-1=(4\pi\rho/Q)\int_0^\infty dr\, r[g(r)-1]\sin(Qr) , \tag{A2}$$

where $S(Q)$ ($g(r)$) stands for either the center of mass or the site-site structure factor (correlation function). In order to apply the convolution theorem, we note that $r[g(|r|)-1]$ is an odd function of r, and therefore the integral in Eq. (A2) can be written as a proper 1D Fourier transform:

$$S(Q)-1=(2\pi i\rho/Q)\int_{-\infty}^{+\infty} dr\, r[g(|r|)-1]\exp(iQr) . \tag{A3}$$

Since $f_2(Q)$, Eq. (3), is simply the 1D Fourier transform of $(1/d)\Lambda(r/d)$, where

$$\Lambda(x)=\begin{cases}1-|x| & \text{for } |x|\le 1\\ 0 & \text{otherwise}\end{cases} \tag{A4}$$

is the triangle function, Eq. (4) follows immediately.

[1] B. J. Berne and D. Thirumalai, Annu. Rev. Phys. Chem. **37**, 401 (1986).
[2] M. P. Allen and D. J. Tildesley, *Computer Simulation of Liquids* (Oxford University Press, Oxford, 1987).
[3] The value of the incoherent cross section of para-hydrogen is similar to the coherent one, when the energy of incoming neutrons is below $\cong 10$ meV. Consequently, the available Q range is limited to $\cong 4.4$ Å^{-1}. However, this range, in the momentum-energy plane, is not sufficient for an exhaustive experimental investigation of the static and dynamic structure factors of liquid hydrogen.
[4] K. Carneiro, M. Nielsen, and J. P. McTague, Phys. Rev. Lett. **30**, 481 (1973).
[5] M. Zoppi, R. Magli, W. S. Howells, and A. K. Soper, Phys. Rev. A **39**, 4684 (1989).
[6] R. Prydz, National Bureau of Standards Report No. 9276, Boulder, CO, 1967 (unpublished).
[7] M. J. Norman, R. O. Watts, and U. Buck, J. Chem. Phys. **81**, 3500 (1984).
[8] Strictly speaking, by changing the density, the corrections to the experimental neutron data will change too, and therefore a new analysis of the raw experimental spectra may be necessary. However, since the corrections are small, this reduces to a second-order effect, which may be neglected within the present accuracy of the experiment.
[9] J. Van Kranendonk, *Solid Hydrogen* (Plenum, New York, 1983).
[10] I. F. Silvera, in *Simple Molecular Systems at Very High Density,* edited by A. Polian, P. Loubeyre, and N. Boccara (Plenum, New York, 1989).
[11] J. D. Poll and M. S. Miller, J. Chem. Phys. **54**, 2673 (1971).
[12] J. P. Hansen and I. R. McDonald, *Theory of Simple Liquids* (Academic, New York, 1986).
[13] N. Metropolis, A. W. Rosenbluth, M. N. Rosenbluth, A. H. Teller, and E. Teller, J. Chem. Phys. **21**, 1088 (1953).
[14] D. Chandler and P. G. Wolynes, J. Chem. Phys. **74**, 4078 (1981).
[15] K. Singer and W. Smith, Mol. Phys. **64**, 1215 (1988).
[16] M. Zoppi and M. Neumann, Phys. Rev. B **43**, 10 242 (1991).
[17] F. Barocchi, M. Neumann, and M. Zoppi, Phys. Rev. A **29**, 1331 (1984).
[18] Since the phase diagram of a *classical* system of particles interacting through the potential of Norman, Watts, and Buck is not known, these other points were obtained by assuming that D_2 may be modeled by a LJ potential with the parameters given in Sec. II and using the critical constants of a classical LJ system [J. J. Nicolas, K. E. Gubbins, W. B. Street, and D. J. Tildesley, Mol. Phys. **37**, 1429 (1979)] as scaling parameters.
[19] G. Jacucci and N. Quirke, Nuovo Cimento B **58**, 317 (1980).
[20] Due to the density between liquid and gas phase, this "average" correlation function is not necessarily normalized to 1.0, asymptotically.
[21] F. Barocchi, M. Neumann, and M. Zoppi, Phys. Rev. A **36**, 2440 (1987).
[22] V. F. Sears, Can. J. Phys. **44**, 1279 (1966).
[23] S. W. Lovesey, *Theory of Neutron Scattering from Condensed Matter* (Oxford University Press, Oxford, 1987), Vol. 1.
[24] This number is obtained by averaging the J-dependent nuclear distances, $d(J)$, for a normal mixture of ortho- and para-deuterium in the vibrational ground state.
[25] A. K. Soper, in *Static and Dynamic Properties of Liquids,* edited by M. Davidovic' and A. K. Soper (Springer-Verlag, Berlin, 1989).
[26] R. L. McGreevy and L. Pusztai, Mol. Sim. **1**, 359 (1988).
[27] M. Zoppi (unpublished).